Wind and Structures, *Vol. 21, No. 2 (2015) 159-182*
DOI: http://dx.doi.org/10.12989/was.2015.21.2.159

Amplitude dependency of damping of tall structures by the random decrement technique

An Xu[1,2], Zhuangning Xie[*1], Ming Gu[1,3] and Jiurong Wu[2]

[1]*State Key Laboratory of Subtropical Building Science, South China University of Technology, Guangzhou, 510641, China*
[2]*Engineering Technology Research and Development Center for Structural Wind Resistance and Health Monitoring in Guangdong Province, Guangzhou University, Guangzhou, 510006, China*
[3]*State Key laboratory for Disaster Reduction in Civil Engineering, Tongji University, Shanghai, 200092, China*

(Received December 23, 2014, Revised April 27, 2015, Accepted May 25, 2015)

Abstract. This study focuses on the amplitude dependency of damping of tall structures by the random decrement technique (RDT). Many researchers have adopted RDT to establish the amplitude dependency of damping ratios in super-tall buildings under strong wind loads. In this study, a series of simulated examples were analyzed to examine the reliability of this method. Results show that damping ratios increase as vibration amplitudes increase in several cases; however, the damping ratios in the simulated signals were preset as constants. This finding reveals that this method and the derived amplitude-dependent damping ratio characteristics are unreliable. Moreover, this method would obviously yield misleading results if the simulated signals contain Gaussian white noise. Full-scale measurements on a super-tall building were conducted during four typhoons, and the recorded data were analyzed to observe the amplitude dependency of damping ratio. Relatively wide scatter is observed in the resulting damping ratios, and the damping ratios do not appear to have an obvious nonlinear relationship with vibration amplitude. Numerical simulation and field measurement results indicate that the widely-used method for establishing the amplitude-dependent damping characteristics of super-tall buildings and the conclusions derived from it might be questionable at the least. More field-measured data must be collected under strong wind loads, and the damping characteristics of super-tall buildings should be investigated further.

Keywords: tall building; wind effect; damping ratio; full-scale measurement; wind-induced vibration; random decrement technique

1. Introduction

Modern tall buildings constructed with high-strength and lightweight materials tend to be more flexible and lightly damped than buildings constructed in the past. As a consequence, these tall buildings display increased sensitivity to dynamic excitation by wind. The response of a structural system to dynamic loading is governed by structural dynamic parameters, such as mass, stiffness, and damping. Unlike mass and stiffness, damping is not related to a unique physical phenomenon. At the design stage, the damping characteristics of building structures are usually assumed in the

*Corresponding author, Professor, E-mail: znxie@scut.edu.cn

http://www.techno-press.org/?journal=was&subpage=8 ISSN: 1226-6116 (Print), 1598-6225 (Online)

dynamic analysis because no widely accepted method to estimate the damping of a structure prior to construction is available at present. Kareem and Gurley (1996) pointed out that the estimation of damping in a structural system is the most difficult problem in structural dynamics. Full-scale measurement of the wind-induced response of super-tall buildings is necessary because the identified damping ratio of a constructed building may be helpful in determining the damping ratios of those in the design stage (Fu *et al*. 2008, 2012, Fukuwa *et al*. 1996, Li *et al*. 1998, 2000, 2003, 2004, Duda *et al*. 1996, Tamura and Suganuma 1996, Wu *et al*. 2007, Yi *et al*. 2013).

Many full-scale measurements of wind effects on super-tall buildings have been carried out in recent years. Damping ratios in super-tall buildings have been identified based on the measured acceleration response. On the basis of field-measured data and identified damping ratios, several researchers have established the point of view that for tall buildings affected by wind loads, the damping ratio is generally nonlinear with respect to the magnitude of the response. Tamura and Suganuma (1996) proposed a modified random decrement technology (RDT) that involves ranking according to peak amplitude to directly evaluate the amplitude dependence of damping ratio. Jeary (1986) discussed nonlinear damping inherent in tall buildings and the mechanism that causes this phenomenon. Li *et al*. (2003) conducted full-scale measurements of wind effects on a 70-storey tall building in Hong Kong and presented the first study in wind engineering that investigates the effects of amplitude-dependent damping on the wind-induced vibration of super-tall buildings. Wu *et al*. (2007) performed full-scale measurements of the wind-induced response of a 79-storey building during the passage of several typhoons and proposed an empirical model of amplitude-dependent damping based on the accumulated measurement results and identified damping data; the dynamic responses of the building predicted with the actual amplitude-dependent damping characteristics were compared with those computed with damping parameters assumed by structural designers to evaluate the adequacy of current design practices and investigate the effects of amplitude-dependent damping on wind-induced responses. Aside from the abovementioned, many other reports on the amplitude-dependent damping characteristics of buildings or structures have been presented (Cele 1996, Fu *et al*. 2012, Jeary 1996, 1997).

A widely accepted fact is that the damping ratio of a tall building is nonlinear with vibration amplitude under strong wind loads. Most amplitude-dependent damping characteristics have been obtained by using the RDT proposed by Cole (1968, 1971), or the modified RDT method proposed by Tamura and Suganuma (1996). The RDT was introduced by Cole for the identification of linear structures subjected to ambient excitation and for the assessment of damage in aircraft structures. The theoretical principle of RDT is based on a conditional expectation. A modified conditional expectation enables RDT to estimate the amplitude-dependent characteristics of buildings and structures. In RDT, the random decrement (RD) functions are estimated by averaging the time segments of the measured signal, which are selected according to certain conditions. The modal parameters of the structures can thus be extracted from the RD functions by fitting the extreme point in the RD functions as an exponential decay curve.

The key step in RDT is to decompose the measured vibration signal into forced and free vibration components. This procedure requires the system to be linear to apply the principle of superposition. Therefore, if structural damping is amplitude dependent and nonlinear, RDT is unsuitable for damping identification in such a system. It is desirable for the method to be widely applicable to nonlinear systems in which the natural frequency and the damping are both amplitude dependent. As mentioned by Tamura and Suganuma (1996), this is one of the reasons for the peak value triggering method proposal. According to this method, peak values are picked up and ranged into several ranks base on order of amplitude, and then the RD signature for each

rank is computed. Finally, the natural frequencies and damping ratios are estimated using the least-squares approximation from the first two periods of each RD signature. The physical meaning of such data processing is clear.

However, the physical meaning of another data processing method is not so clear. In this method, a set of thresholds are used to find segments for obtaining a set of RD signatures with different initial amplitudes. The length of each segment is more than ten times of the period of the corresponding vibration mode. Then regarding the RD signature as a free vibration signal, the damping ratio can be determined using the least-square approximation accordingly. This method was widely used for establishing the amplitude dependency of damping ratio (Wu *et al*. 2007, Fu *et al*. 2008, 2012, Li *et al*. 1998, 2003, 2004, 2008, 2009, Yi *et al*. 2013). It is noteworthy that the method was generally used without examining its validity. This mathematical treatment of a record appears to have no clear physical meaning, and the results derived by it might be unreliable, as will be discussed in the next section.

In this study, a series of simulated signals were utilized to examine the effectiveness of the modified RDT method widely used to establish the amplitude-dependent damping ratio characteristics of tall buildings. Two typical triggering conditions for the RDT method, namely, level crossing and peak value triggering, were considered. The effect of noise on the identified damping ratios was also studied by adding white Gaussian noise to the simulated signals and specifying different signal-to-noise ratios (SNRs). Full-scale measurements of the wind-induced acceleration responses of a super tall building located in South China were then conducted during the passage of four typhoons. The characteristics of the identified damping ratios of the building were presented and discussed. Related results on ambient vibration were also presented for comparison.

2. Review of RDT

RDT, which was introduced by Cole (1968, 1971) at NASA during the late 1960s and early 1970s, is a simple and easy-to-implement method for the analysis of structures loaded with stochastic forces. The relation between the RD signature and the free vibration response is typically derived for the displacement response. The main idea of RDT is to form an ensemble average signature to represent the free vibration response of a system by processing pre-selected segments from measured data. The equation of motion for an under-damped simple system can be formulated as follows

$$\ddot{x}(t) + 2\zeta\omega_n \dot{x}(t) + \omega_n^2 x(t) = F(t) \tag{1}$$

where ω_n and ζ are the undamped natural circular frequency and damping ratio of the system, respectively; $F(t)$ is the generalized excitation of the system; and $\ddot{x}(t), \dot{x}(t), x(t)$ are acceleration, velocity, and displacement at time *t*, respectively. The response of such a system can be expressed as follows

$$x(t) = e^{-\zeta\omega_n t}\left(x(0)\cos\omega_d t + \frac{\dot{x}(0) + \zeta\omega_n x(0)}{\omega_d}\sin\omega_d t \right) + \frac{1}{\omega_d}\int_0^t F(t) e^{-\zeta\omega_n (t-\tau)} \sin\omega_d (t-\tau)\,\mathrm{d}\tau \tag{2}$$

where ω_d is the damped natural circular frequency of the system. Eq. (2) shows that the total

response of the system is due to three factors: initial displacement, initial velocity, and excitation. Theoretically, the dynamic characteristics of the system, including natural frequency and damping ratio, can be obtained by analyzing the RD signature for the displacement response. In order to get the RD signature from a given data, a triggering condition must be specified firstly, and then a series of data segments with the same length can be obtained from the given data by this triggering condition. Finally, the RD signature can be computed by averaging these data segments. In section 3.2 of this paper, two triggering conditions used in this study, including the level-crossing triggering condition and the peak value triggering condition, are introduced in detail.

As shown in Eq. (2), the relationship between the RD signature and the free vibration response is typically derived for the displacement response. However, the acceleration responses of buildings or structures are usually measured in full-scale measurements; achieving an analytical free vibration acceleration response without knowledge of the initial displacement and velocity conditions is thus difficult. Although the RD acceleration signature is not strictly equivalent to the free vibrations of a structure, the equivalence relation between the two can be established approximately in engineering applications (Fu *et al.* 2012, Jeary 1996, Li *et al.* 2000, 2003, 2004, 2007, 2008, 2009; Wu *et al.* 2007, Yi *et al.* 2013); therefore, the measured acceleration data can be directly employed to identify the natural frequencies and damping ratios of buildings and structures through RDT. The identification results of numerical simulations in the next section demonstrate the feasibility of this approach.

The free vibration components of the simple system described in Eq. (1) are as follows

$$x(t)=e^{-\zeta\omega_n t}\left(x(0)\cos\omega_d t+\frac{\dot{x}(0)+\zeta\omega_n x(0)}{\omega_d}\sin\omega_d t\right) \tag{3}$$

$$\dot{x}(t)=e^{-\zeta\omega_n t}\left(\dot{x}(0)\cos\omega_d t-\frac{\zeta\omega_n\dot{x}(0)+\omega_n^2 x(0)}{\omega_d}\sin\omega_d t\right) \tag{4}$$

$$\ddot{x}(t)=e^{-\zeta\omega_n t}\left(\left(-2\zeta\omega_n\dot{x}(0)-\omega_n^2 x(0)\right)\cos\omega_d t+\frac{\zeta\omega_n x(0)+(2\zeta^2-1)\omega_n\dot{x}(0)}{\omega_d}\sin\omega_d t\right) \tag{5}$$

Eq. (5) can be rewritten in a simplified form as

$$\ddot{x}(t)=e^{-\zeta\omega_n t}A\sin(\omega_d t+\varphi) \tag{6}$$

where

$$A=\sqrt{\left(2\zeta\omega_n\dot{x}(0)+\omega_n^2 x(0)\right)^2+\left(\frac{\zeta\omega_n x(0)+(2\zeta^2-1)\omega_n\dot{x}(0)}{\omega_d}\right)^2} \tag{7}$$

$$\varphi=tg^{-1}\frac{-\omega_d\left(2\zeta\omega_n\dot{x}(0)+\omega_n^2 x(0)\right)}{\zeta\omega_n x(0)+(2\zeta^2-1)\omega_n\dot{x}(0)} \tag{8}$$

Natural frequency ω_n and damping ratio ζ can be estimated by fitting the RD signature in the form of Eq. (6) through the least-squares method (i.e., entire curve fitting method). Eq. (6) is

essentially equivalent to the formula with four variables presented by Tamura and Suganuma (1996). A popular and convenient alternative to evaluate damping ratio ζ is to solve the following equation.

$$\zeta = \frac{1}{2\pi j} \ln \frac{\ddot{x}_i}{\ddot{x}_{i+j}} \tag{9}$$

where $\ddot{x}_i$ is the *i*th peak value of the RD signature. The damping ratio of the system can be obtained by fitting the peak value of the RD signature by using a negative exponential function. This method is referred to as peak value fitting method in this study. Both entire curve and peak value fitting methods were utilized to identify the damping ratio. Several selected results are illustrated and discussed.

3. Numerical simulation

3.1 Time series simulation on a specified acceleration spectrum

In the study of Tamura and Suganuma (1996), both the natural frequency and damping ratio of the structure were assumed to be linear with vibration amplitude. The displacement response for damping ratio identification was generated by applying a simulated fluctuating wind force on the structure. The results showed that the damping ratio was overestimated in the high amplitude level and underestimated in the relatively low amplitude level. The error between the identified damping ratio and the preset one should be paid more attention because this error may yield misleading results when this method is employed to identify the damping ratio of an actual building or structure. Another widely utilized method of establishing the amplitude dependence of the damping ratio adopts a concept similar to that of the method of Tamura and Suganuma (1996). The main difference between them is the triggering condition employed in data processing to obtain RD signatures; the former employs the peak value triggering condition, and the latter employs the level-crossing triggering condition.

As mentioned in the first section of this paper, most researchers utilized these methods to analyze field-measured data on super-tall buildings subjected to strong wind loads and establish the amplitude dependence of the damping ratio without examining the validity of these methods. However, most studies have indicated that the amplitude-dependent damping ratio obtained from full-scale measurements of an actual building increases with increasing vibration amplitude. Thus, the following question is presented: is the obtained amplitude-dependent damping ratio the nature of the structures themselves, or at least partly generated by the error when conducting damping ratio identification using the above methods derived from RDT?

In work described in this section, numerical examples were employed to examine the validation of the methods. Unlike the simulation method of Tamura and Suganuma (1996), the time series of acceleration data for analysis were not computed by loading fluctuating wind on a structure with a preset natural frequency and damping ratio, but were directly generated from an acceleration spectrum with preset constant dynamic parameters, including natural frequency and damping ratio. The procedure is described in detail below.

Considering the system expressed in Eq. (1), the Fourier spectral density of its displacement can be evaluated as

$$\begin{aligned} S_{xx}(f) &= \frac{S_{FF}(f)}{\left(\omega_n^2-\omega^2\right)^2+\left(2\zeta\omega_n\omega\right)^2} \\ &= \frac{1}{\omega_n^4}\frac{S_{FF}(f)}{\left(1-\left(\frac{\omega}{\omega_n}\right)\right)^2+\left(2\zeta\frac{\omega}{\omega_n}\right)^2} \\ &= \frac{1}{(2\pi f_n)^4}\frac{S_{FF}(f)}{\left(1-\left(\frac{f}{f_n}\right)^2\right)^2+\left(2\zeta\frac{f}{f_n}\right)^2} \end{aligned} \tag{10}$$

where f and ω denote frequency and circular frequency, respectively; $S_{xx}(f)$ and $S_{FF}(f)$ are the power spectral density of $x(t)$ and $F(t)$, respectively; and f_n and ω_n are the natural frequency and circular natural frequency of the system, respectively. Thus, the power spectral density of the acceleration response of the system can be derived as Eq. (11).

$$S_{\ddot{x}\ddot{x}}(f) = (2\pi f)^4 S_{xx}(f) = \frac{\left(\frac{f}{f_n}\right)^4 S_{FF}(f)}{\left(1-\left(\frac{f}{f_n}\right)^2\right)^2+\left(2\zeta\frac{f}{f_n}\right)^2} \tag{11}$$

The power spectrum of generalized excitation $S_{FF}(f)$ is assumed to be an exponential function of frequency f. This assumption aims to make $S_{FF}(f)$ consistent with the characteristic of actual wind load when f is near the natural frequency for the first mode of the building. Thus, the power spectrum can be formulated as

$$S_{FF}(f) = \eta \cdot f^{\gamma} \tag{12}$$

where η and γ are coefficients depending on the characteristics of wind loads. Substituting Eq. (12) into Eq. (11) yields

$$S_{\ddot{x}\ddot{x}}(f) = \frac{\left(\frac{f}{f_n}\right)^4 \cdot \eta f^{\gamma}}{\left(1-\left(\frac{f}{f_n}\right)^2\right)^2+\left(2\zeta\frac{f}{f_n}\right)^2} = \frac{\frac{\eta}{f_n^4}\cdot f^{\gamma+4}}{\left(1-\left(\frac{f}{f_n}\right)^2\right)^2+\left(2\zeta\frac{f}{f_n}\right)^2} \tag{13}$$

We let $\alpha = \frac{\eta}{f_n^4}$ and $\beta = \gamma + 4$. Eq. (13) can be rewritten as

$$S_{\ddot{x}\ddot{x}}(f)=\frac{\alpha f^{\beta}}{\left(1-\left(\frac{f}{f_0}\right)^2\right)^2+\left(2\zeta\frac{f}{f_0}\right)^2} \tag{14}$$

If the parameters, including α, β, f_0 and ζ are determined, the acceleration response can be obtained in the form of Eq. (14) in the frequency domain. Then, the time series of acceleration can be derived by transforming the acceleration signal from the frequency domain to the time domain using the following equation .

$$\ddot{x}(t)=\sum_{n=1}^{N}\sqrt{2S_{\ddot{x}\ddot{x}}(f)\Delta f}\cos(2\pi ft+\varphi_n) \tag{15a}$$

where t denotes the time instant, $S_{\ddot{x}\ddot{x}}(f)$ is the simulated power spectral density specified by the three sets of parameters illustrated in Table 1, Δf is the frequency interval, ϕ_n is the random phase angle uniformly distributed in the interval of $[0,2\pi]$, N is the length of vector $S_{\ddot{x}\ddot{x}}(f)$, and $\ddot{x}(t)$ is the time series of simulated acceleration.

Eq. (15a) represents a classic approach called harmonic superposition method for the simulation of time series from a specified spectral density. Considering that the original form of the harmonic superposition method usually requires a computer with very large memory and consumes significant computing time for a long time series simulation, Holmes (1978) introduced a more efficient approach for such simulation. In this approach, in order to use the Inverse Fast Fourier Transform (IFFT), Eq. (15(a)) was written in the form of Eq. (15(b)). The expressions in the {} brackets in last row of Eq. (15(b)) represents a complex IFFT of the input vector.

$$\begin{aligned}\ddot{x}(t)&=\sum_{n=1}^{N}\sqrt{2S_{\ddot{x}\ddot{x}}(f)\Delta f}\cos(2\pi ft+\varphi_n)\\&=R\left\{\sum_{n=1}^{N}\sqrt{2S_{\ddot{x}\ddot{x}}(f)\Delta f}e^{i(2\pi ft+\varphi_n)}\right\}\\&=R\left\{\sum_{n=1}^{N}\sqrt{2S_{\ddot{x}\ddot{x}}(f)\Delta f}e^{i\varphi_n}e^{i2\pi ft}\right\}\\&=R\left\{\sum_{n=1}^{N}Z(f)e^{i2\pi ft}\right\}\end{aligned} \tag{15b}$$

where

$$Z(f)=\sqrt{2S_{\ddot{x}\ddot{x}}(f)\Delta f}e^{i\varphi_n} \tag{15c}$$

Given that the constant natural frequency and damping ratio of an ideal acceleration signal can be set in Eq. (14), the simulated time series of the signal contains natural frequency and damping ratio information; that is, the identification results can be compared with the preset values to

examine the effectiveness of the identification method. The correctness of the simulation method shown in Eq. (15(b)) is examined first to ensure the reliability of the subsequent study. The parameters α, β, f_n, and ζ in Eq. (14) are set to 1, 1.7, 0.19, and 1%, respectively, and the sampling frequency and sampling length of the time series were set to 25 Hz and 2^{20}, respectively. Fig. 1 shows the average spectrum of the 100 simulations, and the target spectrum is also presented for comparison. The power spectrum of the simulated signal is in good agreement with the target spectrum. This condition reveals the effectiveness of Eq. (15) for time series simulation. Three sets of acceleration time series were simulated according to the parameters specified in Table 1. In the simulation, the damping ratios are set to 1%, 2%, and 3% in the three cases, and the other parameters, including α, β, and f_n, are unchanged.

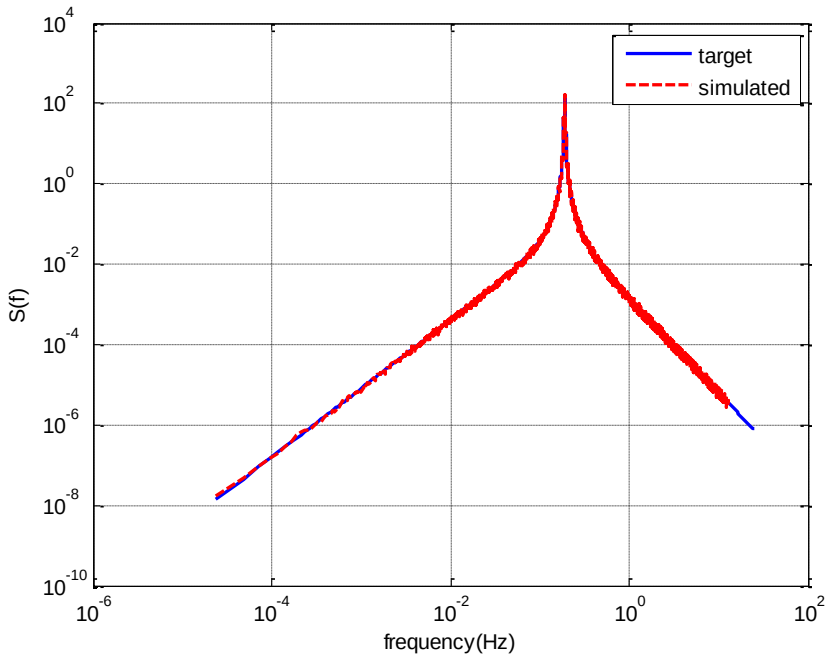

Fig. 1 Comparison of the average spectrum of 100 simulations and the target spectrum

Table 1 Customization of parameters in Eq. (14) for simulation

Case number	α	β	f_n (Hz)	ζ
1	1	1.7	0.19	0.01
2	1	1.7	0.19	0.02
3	1	1.7	0.19	0.03

3.2 Damping ratio identification through RDT

Two different triggering conditions were employed to obtain the RD signatures. One of them was the traditional level-crossing triggering condition, in which the standard deviation of each acceleration response, $\sigma_{\ddot{x}}$, was selected as the triggering level for each sample segment. However, for a discrete time signal, obtaining a precise discrete time t_i in practice is impossible, such that a sampling point $\ddot{x}(t_i)$ crosses the specified triggering level point $\sigma_{\ddot{x}}$. In this case, the triggering condition was modified so that the closest point to the triggering level can be regarded as a starting point for each sample segment. The modified triggering condition is

$$\left[\frac{\left|\ddot{x}(t_i)-\sigma_{\ddot{x}}\right|}{\sigma_{\ddot{x}}}\le 0.05\right]\cap\left[\frac{\left|\ddot{x}(t_i)-\sigma_{\ddot{x}}\right|}{\sigma_{\ddot{x}}}=\min\left(\frac{\left|\ddot{x}(t_k)-\sigma_{\ddot{x}}\right|}{\sigma_{\ddot{x}}}\right)\right](k=i-10,i-9,...,i+9,i+10) \tag{16}$$

Eq. (16) expresses the mathematical functionality of the level-crossing triggering condition, in which $|\cdot|$ and $\cap$ denote the absolute value and the intersection, respectively.

The other triggering condition considered in this study involves selecting a series of peak values from the given data and utilizing them as the starting points of each sample segment (Tamura and Suganuma 1996). This condition is called peak value triggering and can be formulated as

$$\left\{\left[\ddot{x}(t_i)\ge 0\right]\cap\left[\ddot{x}(t_{i-1})\le\ddot{x}(t_i)\right]\cap\left[\ddot{x}(\mathrm{t}_{i+1})\right]\le\ddot{x}(\mathrm{t}_i)\right\}$$

or (17)

$$\left\{\left[\ddot{x}(t_i)\le 0\right]\cap\left[\ddot{x}(t_{i-1})\ge\ddot{x}(t_i)\right]\cap\left[\ddot{x}(t_{i+1})\ge\ddot{x}(t_i)\right]\right\}.$$

In this study the starting point of each sample segment is restricted to the maximum peak of every three sequential peaks from the specified response because the selection of very small peaks may result in a deformed RD signature.

3.2.1 Case of constant damping ratio

For the results described in this section, the damping ratios were assumed to be constant for each case and were identified to verify the performance of RDT. The procedure involves two steps. Firstly, the RD signatures were obtained with both level-crossing and peak value triggering conditions. Secondly, for the RD signature obtained by the above two triggering methods, the natural frequency and damping ratio of the specified data were identified in two ways, namely, (1) fitting the peak values of the RD signature using a negative exponential function and (2) fitting the entire RD signature in the form of Eq. (6). For the level-crossing triggering condition, both the peak value fitting method and the entire curve fitting method were applied. For the peak value triggering method, according to the suggestion by Tamura and Suganuma (1996), only the entire curve fitting method was adopted and only the first two periods of RD signatures were fitted.

The identification results are shown in Table 2. The identified natural frequencies and damping ratios for the three cases are in good agreement with the target values when the level-crossing triggering condition is used. For example, the maximum relative errors of natural frequency and damping ratio identification are approximately 0.16% and 2.00%, respectively. However, when the peak value triggering condition is employed, the maximum relative errors of natural frequency and

damping ratio identification increase to 0.26% and 21.00%, respectively. The reason for this result might be that the accuracy of natural frequency and damping ratio identification depends on the quality of the derived RD signature. Fig. 2(a) shows the derived RD signature using the peak value triggering condition and the fitted function in the form of Eq. (6) for Case 3, and Fig. 2(b) is the corresponding results using the level crossing triggering condition. In order to explain the reason why the level crossing condition gives better identification results, the error between the RD signature and the fitted curve was also plotted. It can be seen that the error between the RD signature and the fitted function is extremely small when using the level crossing triggering condition.

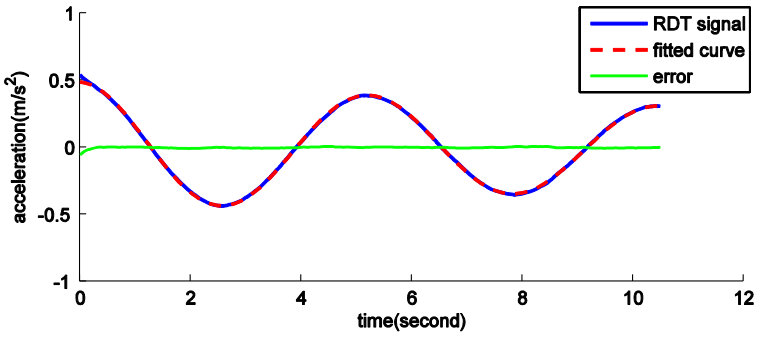

(a)

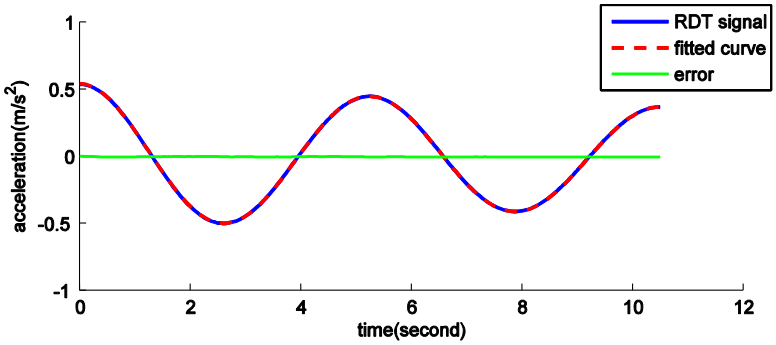

(b)

Fig. 2 Comparison of the RD signature and fitted function for case 3 using (a) the peak value triggering condition and (b) the level crossing triggering condition

Table 2 Identification results obtained by assuming that the damping ratios are constants

Case number		Level crossing triggering condition				Peak value triggering condition	
		Peak value fitting		Entire curve fitting		Entire curve fitting	
		f_0(Hz)	ζ	f_0(Hz)	ζ	f_0(Hz)	ζ
1	value	0.1899	0.0102	0.1899	0.0101	0.1904	0.0113
	error	0.05%	2.00%	0.05%	1.00%	0.21%	13.00%
2	value	0.1897	0.0196	0.1898	0.0200	0.1895	0.0215
	error	0.16%	2.00%	0.11%	0.00%	0.26%	7.50%
3	value	0.1903	0.0305	0.1901	0.0304	0.1899	0.0363
	error	0.16%	1.67%	0.05%	1.33%	0.05%	21.00%

$$* \text{ error} = \left|\frac{\text{identified-target}}{\text{target}}\right| \times 100\%$$

However, the peak value triggering condition produces larger error than the level crossing condition, especially at the start point of the RD signature. This is the very reason why the level triggering method is more accurate at identifying the natural frequency and damping ratio of a system. The base of this conclusion is on the assumption that the damping ratio and natural frequency of a record are constants, and if they are amplitude-dependent for a particular record, the physical meaning of level crossing method is not clear and thus should not be used to establish that dependency.

3.2.2 Amplitude-dependent damping ratio

To the authors' knowledge, the amplitude-dependent damping ratio characteristics of tall buildings under strong wind loads were firstly proposed by Tamura and Suganuma (1996). Many other researchers have reported similar results from full-scale measurements since then (Wu *et al.* 2007, Fu *et al.* 2008, 2012, Li *et al.* 1998, 2003, 2004, 2008, 2009, Yi *et al.* 2013). In the study of Tamura and Suganuma (1996), the peak value triggering method was used to get the RD signature from a particular record, and the first two periods of RD signature were used to identify the natural frequency and damping ratio of a system by fitting an equation with four variables. For a specified rank, a set of natural frequency and damping ratio was identified. If a series of ranks were specified in different vibration amplitudes, a series of RD signatures can be obtained and then a series of natural frequencies and damping ratios can be identified. The amplitude dependency of natural frequency and damping ratios in buildings or structures can be established according to the aforementioned procedure. This method is of clear physical meaning and technically sound. However, just as described in the previous section, this method may produce relatively large errors in some situations due to insufficient quality of RD signatures, as has been discussed in the previous section.

Some other researchers adopted the level crossing triggering method to establish the amplitude dependency of damping. For example, in the study of Yi *et al*. (2013), a set of thresholds were used to find segments for obtaining a set of RD signatures with different initial amplitudes, and the length of each segment was more than ten times of the period of the corresponding vibration mode. In that study, the adopted triggering condition and the fitting method (peak value fitting or entire curve fitting) were not clearly explained, meanwhile the entire RD signature of over ten periods was used to identify the damping ratio. If the peak value triggering method was used in this study, they should follow the conclusion by Tamura and Sugnuma (1996) that only first two periods of RD signature can be used to identify the natural frequency of damping ratio. Obviously the study of Yi *et al*. (2013) did not follow that conclusion. Therefore, the level crossing triggering condition with a set of thresholds might be used in the study of Yi *et al.* (2013). The physical meaning of this mathematical treatment of the initial condition is not clear. This data processing method was adopted by some other researchers (Fu *et al*. 2008, 2012, Li *et al*. 2004, 2008, 2009) without examining its validity.

In this section, the level crossing triggering method for establishing the amplitude dependency of damping ratio was examined by applying it to a set of simulated records. Given that the damping ratios are specified as constants for the three cases stated above, the identification results should be amplitude-independent. The detailed procedure is described as follows.

The amplitude-dependent damping ratios were established by specifying the level-crossing value from $0.02\sigma_{\ddot{x}}$ to $1.0\sigma_{\ddot{x}}$ with a step length of 0.02 $\sigma_{\ddot{x}}$, in which $\sigma_{\ddot{x}}$ denotes the standard deviation of the given signal. For each RD signature, the sample length is set to 500. Thus, the sample time is 20 s or about 3.8 periods of the simulated signal. The result of a typical example, case 3, is shown in Fig. 3(a). It is seen that both peak value and entire curve fitting methods are unable to provide good results when the vibration amplitudes are low; however, when the vibration amplitudes are relatively high, the identification results are of high precision. Similar results were obtained from other cases, and they are not presented in this paper for brevity.

To explain this phenomenon, a dimensionless number, shown in Eq. (18), is introduced to profile the relative error between the RD signature and the fitted function in the form of Eq. (6).

$$E = 1 - \frac{(\phi_R^T \phi_f)^2}{(\phi_R^T \phi_R)(\phi_f^T \phi_f)} \tag{18}$$

where ϕ_R and ϕ_f are the RD signature and fitted function in the form of a column vector, respectively, and $(\bullet)^T$ denotes the transposition. The above definition is for the entire curve fitting method. For the peak value fitting method, ϕ_R and ϕ_f are the real peak values of the RD signature and fitted peak values, respectively. Since the RD signature is derived from the measured acceleration data, ϕ_R and ϕ_f are vectors of accelerations here.

The relative error between the peak values of the RD signature and the fitted peak values for case 3 is shown in Fig. 3(b). Obviously the number *E* describes the degree of reliability of the identified damping ratios. A small *E* indicates high reliability of the identified damping ratio. The above analysis shows that the reliability of the identified damping ratios at low amplitude is very low, and the unreliable results can't properly represent the characteristics of damping ratios in super-tall buildings under wind loads. When the entire curve fitting method is employed, similar results are obtained. Disregarding unreliable identification results at low amplitude levels might

give misleading results when evaluating the damping ratios of actual tall buildings from field-measured acceleration data. As will be seen in the next section, random noise in records can make the identification results even worse.

3.2.3 Influence of random noise on damping ratio identification

The simulated signal utilized in the previous section is a type of signal that contains no noise component; however, the field-measured acceleration signal usually contains noise. In this section, the influence of noise on the accuracy of damping ratio identification was studied. Acceleration data containing noise were generated by adding white Gaussian noise to the simulated signal used previously. A scalar signal-to-noise (SNR) was employed to specify the SNR for each sample in dB.

The SNR was specified as 20, 10, and 5 dB for each case to observe the influence of signal noise on the accuracy of damping ratio identification. Only the results of case 2 are presented for brevity. Figs. 4(a)-4(c) show the identified damping ratios of the simulated signals containing noise with different SNRs. The identified damping ratios appear to increase nonlinearly with the increase in vibration amplitude. These results reveal that the noise in signals might cause serious misinterpretation of the characteristics of damping ratios in buildings; that is, the customized damping ratio is a constant for each sample, whereas the identification results increase nonlinearly with vibration amplitude.

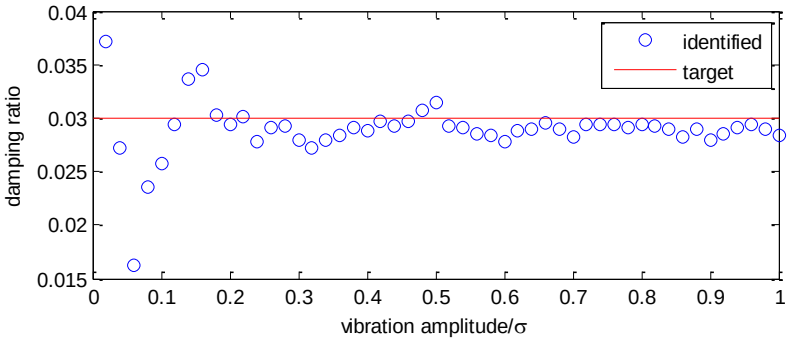

(a)

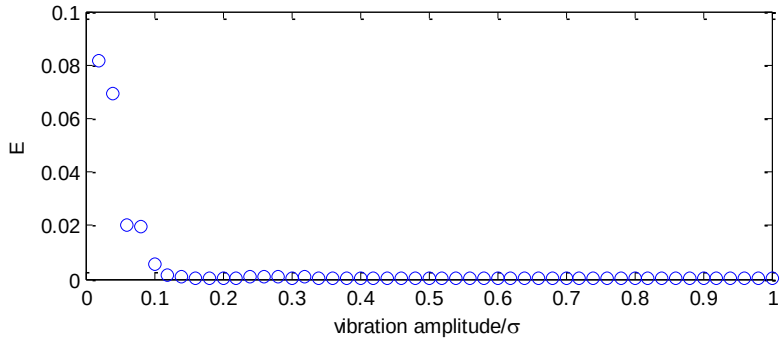

(b)

Fig. 3 (a) Obtained amplitude-dependent damping ratio for case 3 and (b) the corresponding relative error

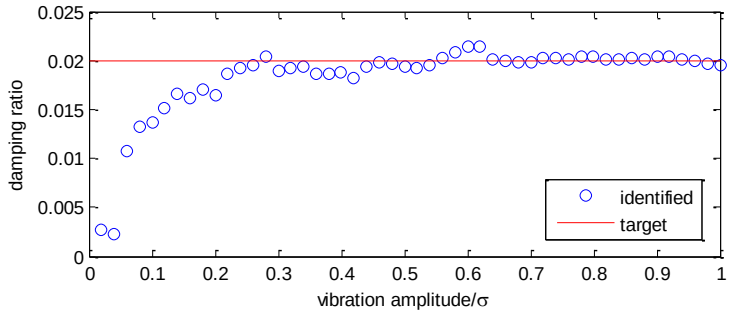

(a)

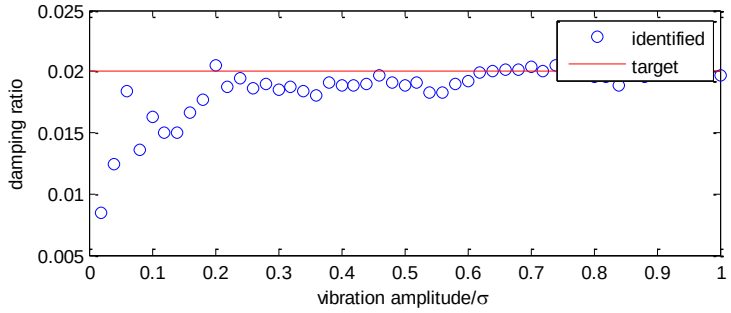

(b)

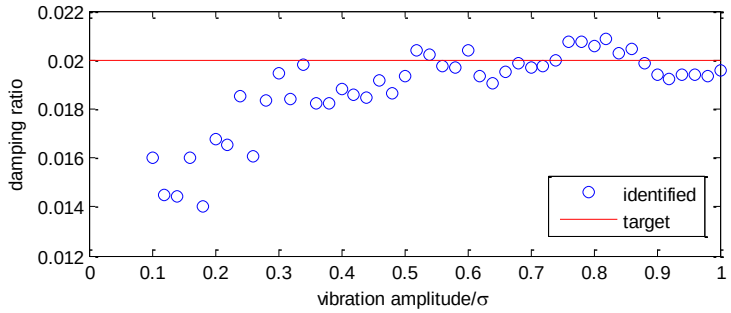

(c)

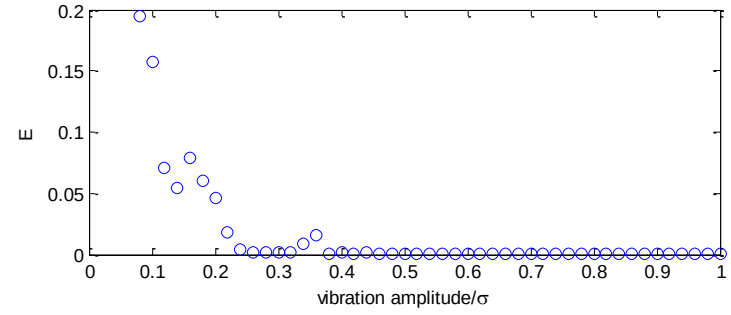

(d)

Fig. 4 (a) Idenfication results for case 2 with SNR equaling to 20 dB (b) with SNR equaling to 10 dB (c) with SNR equaling to 5dB and (d) relative error corresponding to (c)

The corresponding relative errors plotted in Fig. 4(d) show why the misleading results are obtained, that is, the identified damping ratio for low amplitude level is unreliable. It can also be seen that the crossing level as large as root-mean-square (RMS) acceleration is appropriate for accurate damping estimation. Therefore, this threshold value was used to identify the natural frequency and damping ratio of an actual building, as will be seen in the next section.

4. Damping ratio characteristics of an actual building

To obtain the damping ratio characteristics of an actual super-tall building, field measurements of wind-induced acceleration were conducted on Zhuoyue Century Center (ZCC) during the period when the building was affected by four violent typhoons from 2011 to 2013.

ZCC is 280 m high with 68 stories, and is located in Shenzhen, China. A wireless accelerometer (Type LAC-I) was installed on the 68th floor to monitor the acceleration response along the two main axes of the building, as shown in Figs. 5(a) and 5(b). The LAC-I accelerometer, developed by the project team, can record the acceleration signals continuously at a measuring range of ±128 milli-g and a resolution of less than 2 μg, as shown in Fig. 5(c). This type of accelerometer has been designed especially for the measurement of wind-induced vibration of buildings and structures, and its appropriate measuring range guarantees recorded data with a high SNR. The LAC-I accelerometer sends the recorded data to the main computer through a GPRS network serviced by China Mobile Communications Corporation. If the network connection is interrupted, the data will be stored in the flash memory and sent to the main computer automatically when network connection is recovered. These features allow users to remotely monitor the acceleration of buildings or structures conveniently.

The four typhoons stated above include Typhoon Nesat in 2011, Typhoon Doksuri and Typhoon Vicente in 2012, and Typhoon Usage in 2013. For the passage of each typhoon, four or five segments of acceleration data were used to identify the damping ratio of the building. Each segment contains the acceleration response of ZCC during 2 h. Four segments of acceleration response data under ambient excitation were also measured and analyzed for comparison. All data were measured at a frequency of 25 Hz. The time histories of the section of acceleration data with the maximum vibration amplitude measured during each typhoon's passage are illustrated in Figs. 6-9.

The recorded maximum wind-induced acceleration response was approximately 11.0 milli-g during Typhoon Vicente in 2012. To the authors' knowledge, the observed maximum acceleration of super-tall buildings under wind loads rarely exceeds 10 milli-g. Hence, the measured data are very valuable for the study of the damping characteristics of super-tall buildings under strong wind loads.

The data from the full-scale measurements were utilized to observe the relationship between the damping ratio and the vibration amplitude. Since the amplitude dependent behaviors of natural frequency and damping ratio are closely related and cannot be separated (Jeary 1986), the identification results of natural frequency are also presented and discussed.

As discussed in the previous section, the method that employs different threshold values for RDT to evaluate the relationship between the damping ratios and vibration amplitudes is unreliable. Therefore, a simple and direct method was adopted in this study. That is, the damping ratio of each segment was identified by using the level-crossing triggering condition, in which the threshold value was specified as the standard deviation of the data segment. Given that the standard

deviation of each data segment is different, the relationship between natural frequencies, damping ratios and vibration amplitudes can be established from the identification results of more than 20 data segments. The detailed steps are as follows.

(I) The components not related to the fundamental mode were removed using a band pass filter that accepts frequencies within the specified range of $[(1-25\%)f_n,(1+25\%)f_n]$ and rejects frequencies beyond this range.

(II) A crossing level of $1.0\sigma_{\ddot{x}}$, where $\sigma_{\ddot{x}}$ is the standard deviation of the current section of the recorded acceleration data, was specified.

(III) The RD signature was obtained by using the level-crossing triggering condition.

The natural frequency and damping ratio of the current data segment were estimated with peak value fitting method, and the identified damping ratio is plotted against vibration amplitude, which is expressed by $\sigma_{\ddot{x}}$.

The identified damping ratio against the vibration amplitude was plotted in Fig. 10. Different symbols denote the results from different typhoons or ambient excitation cases. It can be seen that the identified natural frequency of the ZCC decreases with the increasing vibration amplitude in a very narrow range. The regularity is similar to that obtained by Tamura and Suganuma (1996). The relationship between the identified damping ratios and the corresponding vibration amplitudes is illustrated in Fig 11. The identified damping ratios of ZCC vary from 0.0053 to 0.0132 in *x* direction and from 0.0042 to 0.0093 in *y* direction. Fig. 12 shows the corresponding identification error of Figs. 10 and 11.

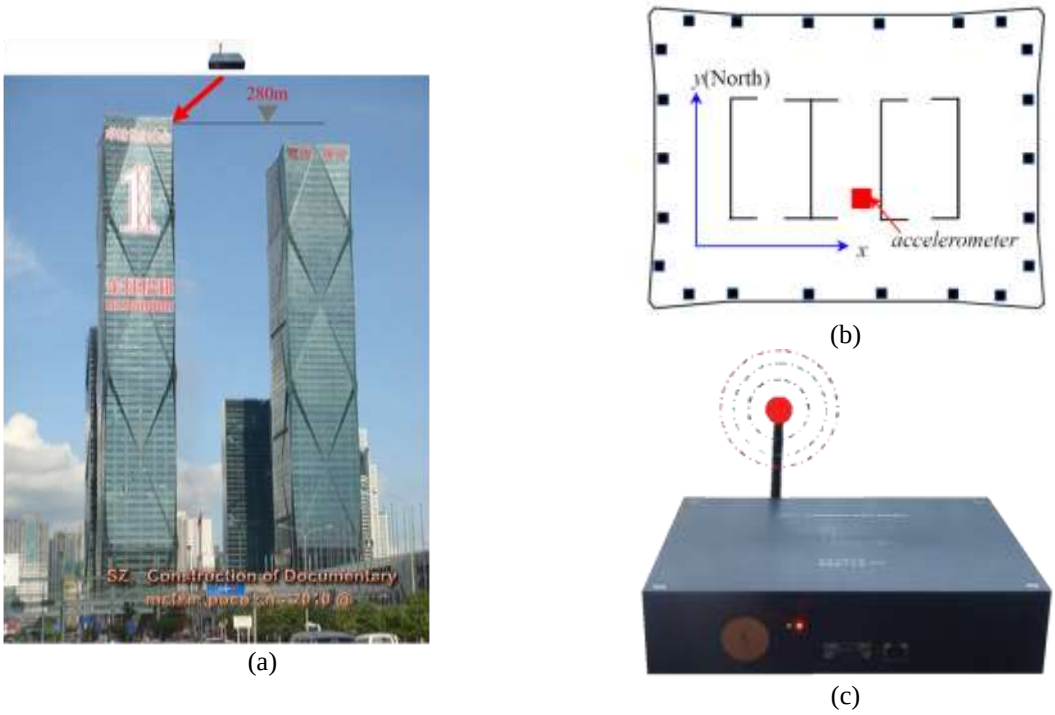

(a) (b) (c)

Fig. 5 (a) Image of the building and height of the accelerometer (b) Accelerometer installed along the two main axes of ZCC and (c) LAC-I wireless accelerometer developed by the project team

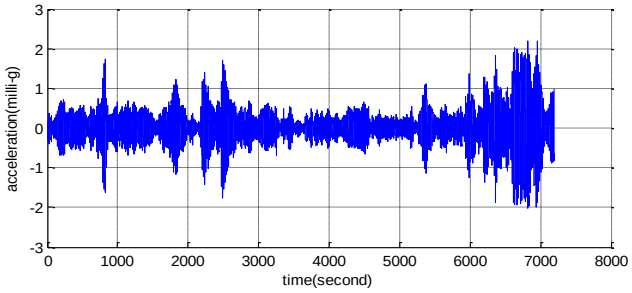

(a)

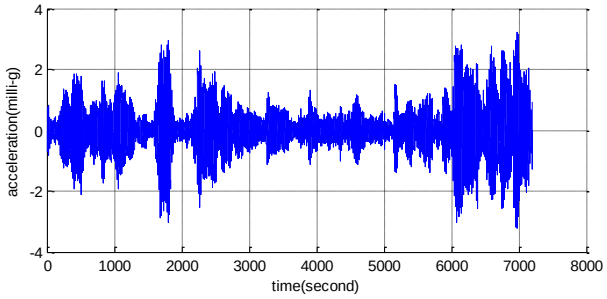

(b)

Fig. 6 Acceleration response during Typhoon Nesat in (a) *x* direction and (b) *y* direction

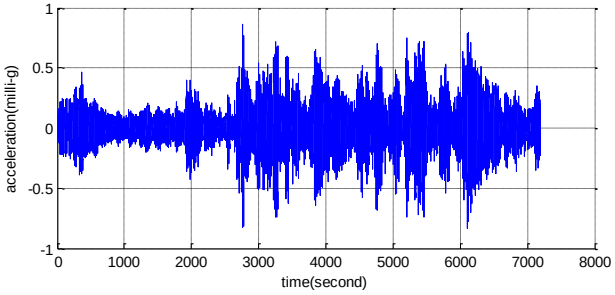

(a)

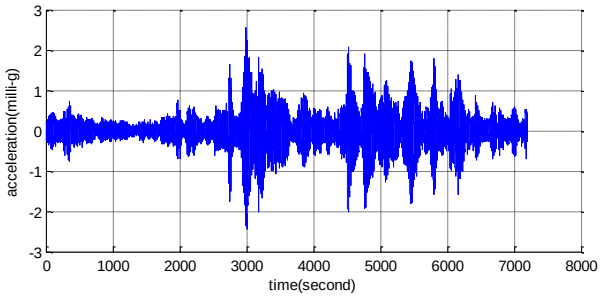

(b)

Fig. 7 Acceleration response during Typhoon Doksuri in (a) *x* direction and (b) *y* direction

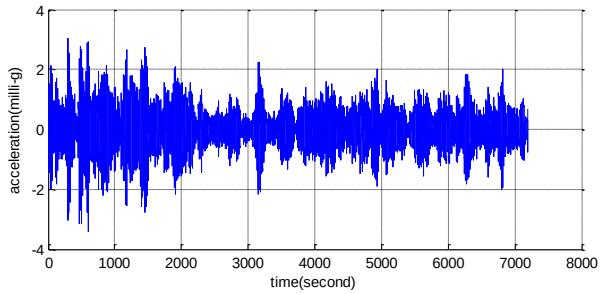

(a)

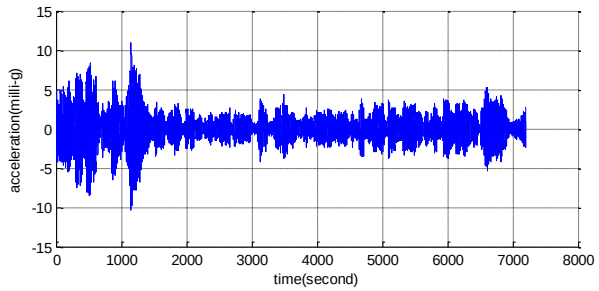

(b)

Fig. 8 Acceleration response during Typhoon Vicente in (a) *x* direction and (b) *y* direction

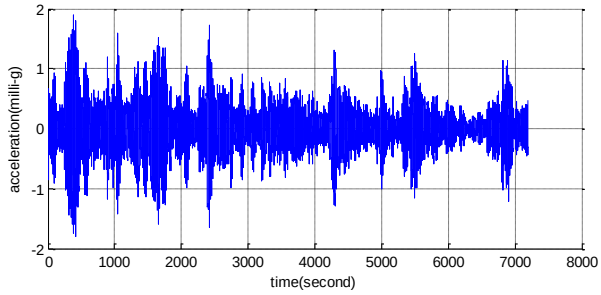

(a)

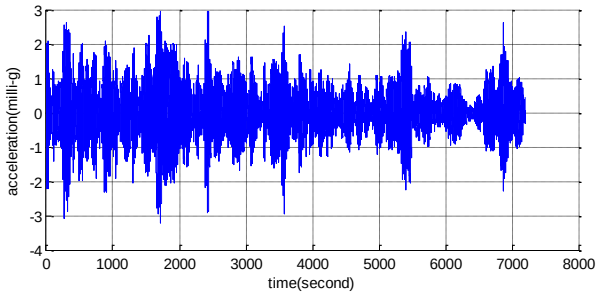

(b)

Fig. 9 Acceleration response during Typhoon Usage in (a) *x* direction and (b) *y* direction

The trend is similar to that of the numerical simulation in the previous section; that is, the relative error is large when the vibration amplitude is relatively low. This finding reveals that the identification results from data with low amplitude are unreliable. The identified damping ratios scatter in a relatively wide range but appear to have no obvious nonlinear relationships with vibration amplitude. At least, the tendency in Fig. 11 is totally different from the reported results in some literatures (Wu *et al*. 2007, Fu *et al*. 2008, 2012, Li *et al.* 1998, 2003, 2004, 2008, 2009, Yi *et al.* 2013).

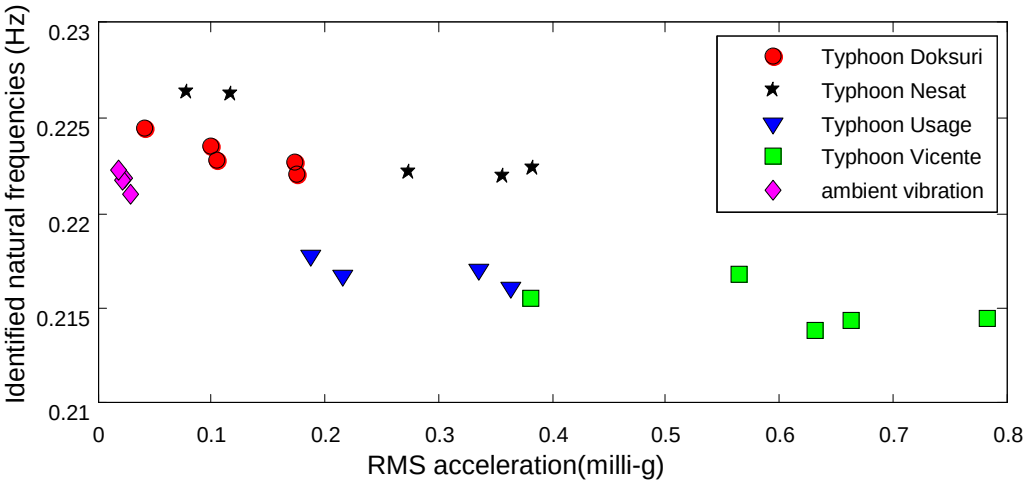

(a)

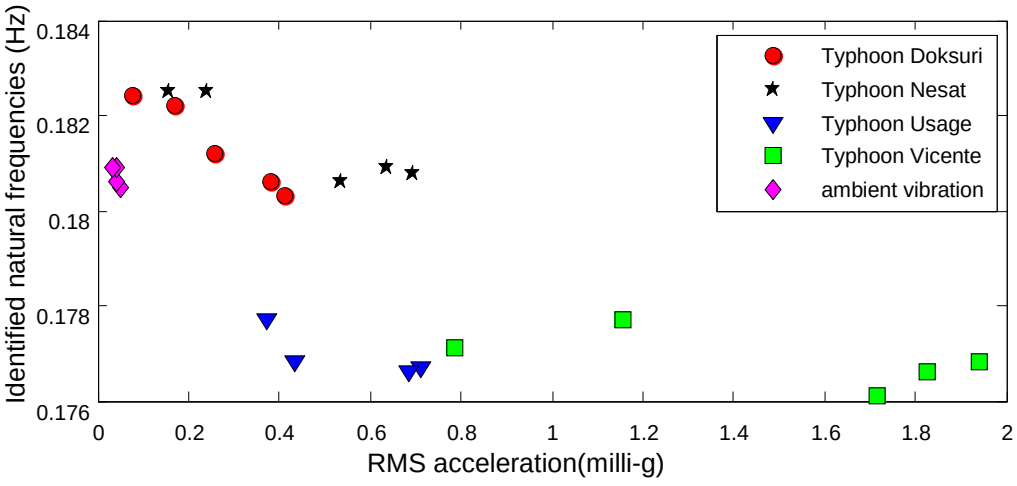

(b)

Fig. 10 Relationship between identified natural frequencies and vibration amplitudes in (a) *x* direction and (b) *y* direction

The reason for the dispersion of the identified damping ratios under different load cases may be that the field-measured acceleration data still contain noise even though the data are filtered before analysis; therefore, the insufficient quality of the derived RD signature could have caused errors in damping ratio identification. Consequently, the identified damping ratios obtained from full-scale measurements provide an approximate range but not an exact value of the real damping ratio of the building.

But in general, the recorded data and the derived RD signatures in this study are of high quality. One example is the RD signature derived from the recorded signal with maximum vibration amplitude during typhoon Vicente (Fig. 13). The decay curve is highly smoothed, and the extreme points of the decay curve almost lay on the fitted negative exponential function. Therefore, the obtained damping ratio results provide a good reference for researchers and engineers involved in structural design and wind engineering.

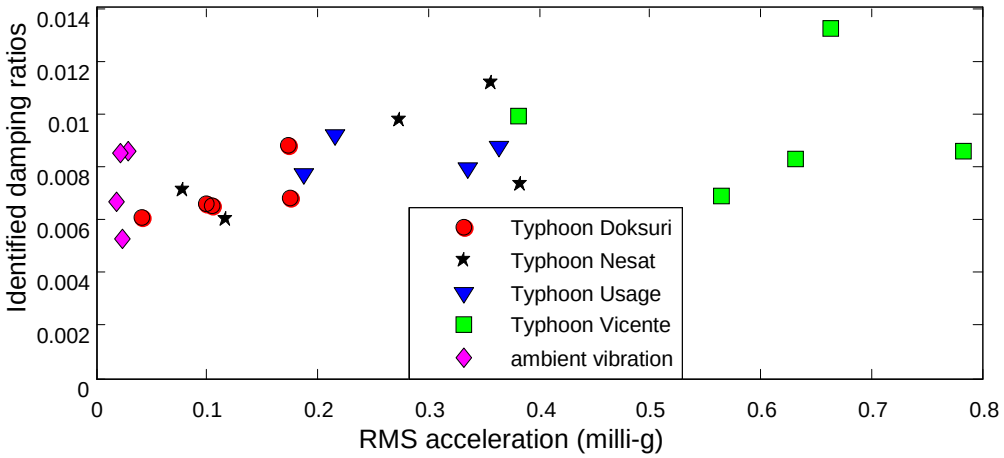

(a)

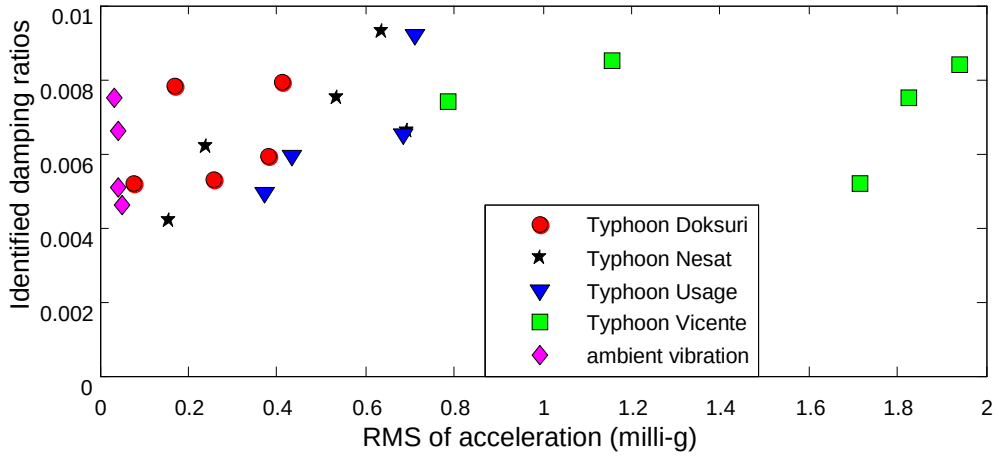

(b)

Fig. 11 Relationship between identified damping ratios and vibration amplitudes in (a) *x* direction and (b) *y* direction

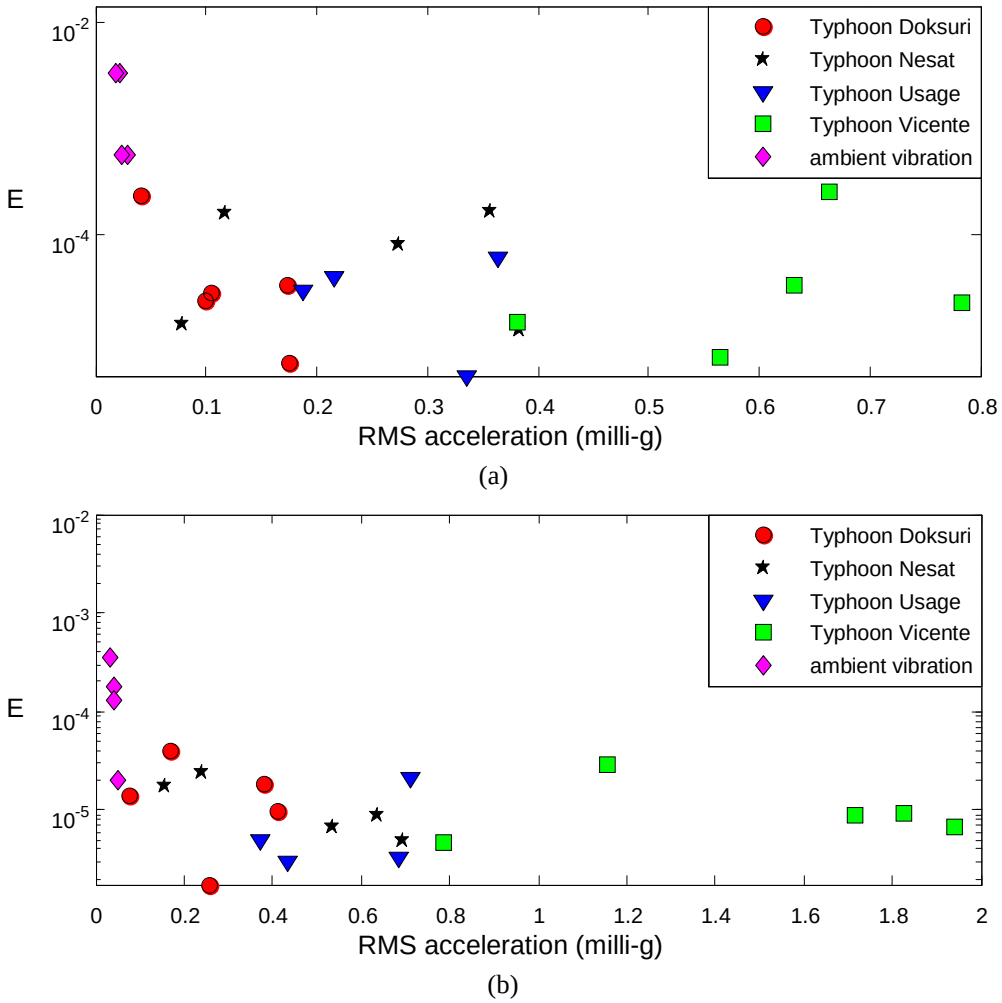

Fig. 12 Relative error between the peak value of the RD signature and the fitted peak value in (a) *x* direction and (b) *y* direction

Both the results from numerical simulation and field-measured data in this study demonstrated that the RDT can give reliable damping ratio identification results at high amplitudes of vibration, so this technique is suitable for damping ratio identification by specifying an appropriate triggering condition level, for instance, the standard deviation of the given data. Conversely, the technique can give significant errors at low amplitudes of vibration, and therefore, the obtained results for low amplitudes of vibration are unreliable. Since the vibration amplitude (generally RMS acceleration) usually starts from a very small value in many studies of the amplitude dependency of damping (Fu *et al.* 2008, 2012, Li *et al.* 2004, 2008, 2009, Yi *et al*. 2013), the damping identification results in these literatures are questionable at the least.

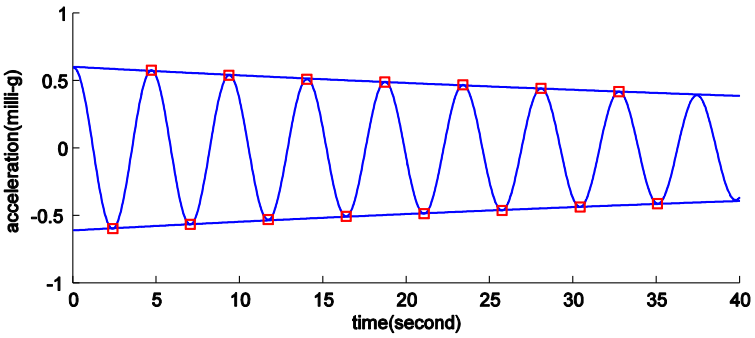

(a)

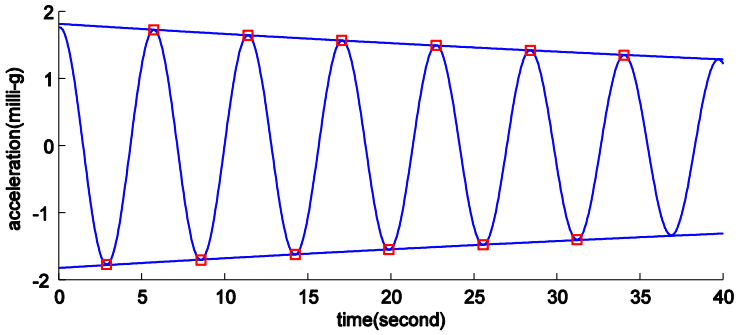

(b)

Fig. 13 RD signature and the fitted negative exponential function of the largest-amplitude data segment in (a) *x* direction and (b) *y* direction

5. Conclusions

This study has focused on the amplitude dependency of damping of tall structures by RDT. A series of simulated signals were generated to verify the effectiveness of the modified RDTs for establishing the amplitude dependence of damping ratios of super-tall buildings. The numerical simulations reveal that the level crossing method with different thresholds for establishing the amplitude-dependent damping characteristics of tall buildings can produce misleading results; that is, the actual damping ratio of the system is specified as a constant, but the identification results are amplitude dependent in several cases. Moreover, these methods obviously yield misleading results when the signals contain noise components. Therefore, the methods and the amplitude-dependent damping models derived from them are questionable at the very least. On the other hand, the peak value triggering method is appropriate for dynamic parameters identification

of a nonlinear system, but in some situation, the insufficient quality of the derived RD signature may cause relatively large error.

Field-measured data obtained from a super-tall building (ZCC) during the passage of four typhoons were utilized to observe whether the damping ratio of the building is amplitude dependent or not. The results obtained with a simple and direct method show that the damping ratio of ZCC varies from 0.0053 to 0.0132 in *x* direction and from 0.0042 to 0.0093 in *y* direction. The identified damping ratios scatter in a relatively wide range, and seem to increase very slightly with the increasing vibration amplitude, but the dependency is not very clear, or at least the tendency is quite different from some other reports adopting multi-triggering-levels (Fu *et al.* 2008, 2012, Li *et al*. 2004, 2008, 2009, Yi *et al*. 2013). The relative error figures indicate that the results are unreliable when the vibration amplitudes are low. Thus, establishing an amplitude-dependent model based on these identification results is not feasible.

As pointed out by many researchers, the damping phenomenon is one of the most difficult problems in dynamics. Since the damping of a tall structure is complicated and not clearly known, there is no theoretical method for estimating damping in buildings (Tamura 2012). More field-measured data on super-tall buildings under strong wind loads should be accumulated, and more studies on the damping characteristics of these buildings should be conducted.

Acknowledgements

The research described in this paper was financially supported by grants from the National Science Foundation of China (51278204, 51208127, and 51478130), the Natural Science Foundation of Guangdong Province, China (S2012010009831), and the Project of Science and Technology of Guangzhou, China (2014J4100141). The authors gratefully acknowledge such financial support.

References

Aquino, R.E. and Tamura, Y. (2013), "Framework for structural damping predictor models based on stick-slip mechanism for use in wind-resistant design of buildings", *J. Wind Eng. Ind. Aerod.*, **117**, 25-37.

Cele, M. (1996), "Comparison of damping in buildings under low-amplitude and strong motions", *J. Wind Eng. Ind. Aerod.*, **59**, 309-323.

Cole, H.A. (1971), Method and apparatus for measuring the damping characteristics of a structure, *United States Patent* No. 3, 620, 069.

Cole, H.A. (1968), "On-the-line analysis of random vibrations", AIAA Paper No. 68-288, AIAA/ASME Structures, *Structural Dynamics and Material Conference*, Palm Springs.

Duda, K., Satake, N., Ono, J. and Sasaki, A. (1996), "Damping properties of buildings in Japan", *J Wind Eng. Ind. Aerod.*, **59**(2-3), 383-392.

Davenport, A.G. and Carroll, H. (1986), Damping in tall buildings: its variability and treatment in design. ASCE Spring Convention, Seattle, 42-57.

Fu, J.Y., Li, Q.S., Wu, J.R., Xiao, Y.Q. and Song, L.L. (2008), "Field measurements of Boundary layer wind characteristics and wind-induced responses of super-tall buildings", *J. Wind Eng. Ind. Aerod.*, **96**(8-9), 1332-1358.

Fu, J.Y., Wu, J.R., Xu, A., Li, Q.S. and Xiao YQ. (2012), "Full-scale measurements of wind effects on Guangzhou West Tower", *Eng. Struct.*, **35**, 120-139.

Fukuwa, N., Nishizaka, R., Yagi, S., Tanaka, K. and Tamura, Y. (1996), "Field measurement of damping and

natural frequency of an actual steel-framed building over a wide range of amplitudes", *J. Wind Eng. Ind. Aerod.*, **59**(2-3), 325-347.
Holmes, J.D. (1978), "Computer simulation of multiple, correlated wind records using the inverse Fast Fourier Transform", *Civil Eng. Trans., Institution of Engineers, Australia*, **20**(1), 67-74.
Jeary, AP. (1986), "Damping in tall buildings, a mechanism and a predictor", *Earthq. Eng. Struct. D.*, **14**(5), 750-773.
Jeary, A.P. (1996), "The description and measurement of nonlinear damping in structures", *J. Wind Eng. Ind. Aerod.*, **59**(2-3), 103-114.
Jeary, A.P. (1997), "Damping in structures", *J. Wind Eng. Ind. Aerod.*, **72**, 345-355.
Kareem, A. and Gurley, K. (1996), "Damping in structures: its evaluation and treatment of uncertainty", *J. Wind Eng. Ind. Aerod.*, **59**(2-3), 131-157.
Li, Q.S., Fang, J.Q., Jeary, A.P. and Wong, C.K. (1998), "Full scale measurement of wind effects on tall buildings", *J. Wind Eng. Ind. Aerod.*, **74-76**, 741-750.
Li, Q.S., Liu, D.K., Fang, J.Q., Jeary, A.P. and Wong, C.K. (2000), "Damping in buildings: its neural network and AR model", *Eng. Struct.*, **22**(9), 1216-1223.
Li, Q.S., Yang, K., Wong, C.K. and Jeary, A.P. (2003), "The effect of amplitude-dependent damping on wind-induced vibrations of a super tall building", *J. Wind Eng. Ind. Aerod.*, **91**(9), 1175-1198.
Li, Q.S., Xiao, Y.Q., Wong, C.K. and Jeary, A.P. (2004), "Field measurements of typhoon effects on a super tall building", *Eng. Struct.*, **26**(2), 233-244.
Li, Q.S., Xiao, Y.Q., Fu, J.Y. and Li, Z.N. (2007), "Full-scale measurements of wind effects on the Jin Mao Building", *J. Wind Eng. Ind. Aerod.*, **95**(6), 445-466.
Li, Q.S., Xiao, Y.Q., Wu, J.R., Fu, J.Y. and Li, Z.N. (2008), "Typhoon effects on super-tall buildings", *J Sound Vib.*, **313**(3-5), 581-602.
Li, Q.S., Wu, J.R., Fu, J.Y., Li, Z.N. and Xiao, Y.Q. (2009), "Wind effects on the world's tallest reinforced concrete building", *Struct. Build.*, **163**(2), 97-110.
Tamura, Y. and Suganuma, K. (1996), "Evaluation of amplitude-dependent damping and natural frequency of buildings during strong winds", *J Wind Eng. Ind. Aerod.*, **59**(2-3), 115-130
Tamura, Y. (2012), "Amplitude dependency of damping in buildings and critical tip drift ratio", *Int. J. High-Rise Build.*, **1**, 1-13.
Wu, J.R., Liu, P.F. and Li, Q.S. (2007), "Effects of amplitude-dependent damping and time constant on wind-induced responses of super tall building", *Comput. Struct.*, **85**(15-16), 1165-1176
Yi, J, Zhang, J.W., and Li, Q.S. (2013), "Dynamic characteristics and wind-induced responses of a super-tall building during typhoons", *J Wind Eng. Ind. Aerod.*, **121**, 116-130.

JH